

Mutual diffusion in a binary Ar-Kr mixture confined within zeolite NaY

C. R. Kamala

Solid State and Structural Chemistry Unit, Indian Institute of Science, Bangalore, India

K. G. Ayappa

Department of Chemical Engineering, Indian Institute of Science, Bangalore, India

S. Yashonath

Solid State and Structural Chemistry Unit and Supercomputer Education and Research Center, Indian Institute of Science, Bangalore, India

(Received 15 February 2002; published 21 June 2002)

Molecular dynamics investigations of the mutual diffusion coefficients in an Ar-Kr mixture confined in the zeolite NaY are reported. Velocity auto- and cross correlations were computed at two different temperatures (200 and 600 K). The importance of the appropriate choice of reference frame while evaluating the time correlation functions is illustrated for argon in the zeolite NaY. Mutual diffusivities in the mixture were obtained in the barycentric reference frame. Recently, Zhou and Miller showed that the distinct diffusivity \mathcal{D}_d is zero for the Ar-Kr mixture in bulk. On confinement, it is seen that at 200 K the ratio $R = \mathcal{D}_{11}/\mathcal{D}_s = 0.77$, where \mathcal{D}_{11} is the mutual diffusivity and \mathcal{D}_s is the mixture self-diffusivity. However, at 600 K, $R = 0.97$, implying that the contribution from distinct diffusion is only slightly negative. The large negative \mathcal{D}_d at 200 K could be attributed to strong localization of Ar and Kr in the physisorption sites within the zeolite cages. Analysis of error bars and an efficient computational algorithm for evaluation of the velocity cross correlation function are also presented. The results have implications in biology, chemistry, and other situations where transport of confined mixtures is encountered.

DOI: 10.1103/PhysRevE.65.061202

PACS number(s): 66.30.Ny, 82.75.Mj, 61.20.Ja, 02.70.Ns

I. INTRODUCTION

During the past two decades, the study of the properties of molecularly confined fluids has attracted much attention [1,2], since fluids are often found confined within another medium. Examples of this kind abound in both the pure and applied sciences; molecules and ions within membranes and blood within capillaries being typical examples from the biological sciences, while boundary lubrication and superionic conductors are examples from engineering and physics. Catalytic reactions within porous solids and inclusion compounds are instances from chemistry. Due in part to the strong interaction with the confining host, confined fluids generally exhibit properties that are different from those of bulk fluids. Single file diffusion, dependence of self-diffusivity on concentration, and the levitation effect are a few examples where confined fluids show interesting behavior [2].

Zeolites are microporous materials whose pore dimensions are comparable to the size of the molecules typically confined within them [3]. They are an important class of solids used industrially for catalysis, molecular sieving, and ion exchange. One of the most common uses of zeolites is for separation of hydrocarbon and other mixtures. Understanding the dynamics of molecular mixtures confined within the zeolitic pores at a fundamental level is expected to enhance our understanding of the molecular sieving property of zeolites. Although transport properties of mixtures have been investigated for bulk fluids, the deviation of these properties for ideal and nonideal mixtures under confinement has received much less attention. In this work, we focus our atten-

tion on calculating diffusion coefficients for binary mixtures confined within a zeolite, using molecular dynamics (MD) simulations. Although experimental techniques such as pulsed field gradient NMR and neutron scattering have yielded some insight into the dynamics of molecules confined within the zeolite pores, our understanding is still far from complete [1].

The foundations for the statistical mechanical treatment and molecular theory of diffusion of multicomponent mixtures were laid by Bearman and Kirkwood [4,5]. These as well as more recent studies on single component and binary mixtures of bulk fluids compute time correlation functions such as the velocity autocorrelation function (VACF)

$$C(t) = \langle \mathbf{v}_i(\tau) \cdot \mathbf{v}_i(\tau+t) \rangle_{\tau,N} \quad (1)$$

and the velocity cross correlation function (VCCF)

$$C_c(t) = \langle \mathbf{v}_i(\tau) \cdot \mathbf{v}_j(\tau+t) \rangle_{\tau,N}, \quad (2)$$

which are used to calculate the transport properties of fluids within the framework of equilibrium statistical mechanics. Here \mathbf{v}_i is the velocity of the i th particle. The structure of the VCCF has been analyzed for Lennard-Jones (LJ) liquids, soft spheres [6–9], liquid rubidium, and other single component fluids [10] using MD simulations. In these studies investigations into the contributions from the first, second, and higher shells to the total VCCF give insight into the mechanism of momentum transfer in these systems. Unlike self-diffusivities, which require only the VACF, computations of the mutual diffusivity (\mathcal{D}_{11}) (also referred to as the chemical diffusivity) in multicomponent mixtures require a

knowledge of the VCCFs as well. The contribution to the mutual diffusivity \mathcal{D}_{11} from the VCCFs is referred to as the distinct diffusivity \mathcal{D}_d . It has contributions from the VCCFs of both like and unlike species. The mixture self-diffusivity \mathcal{D}_s is a linear combination of individual self-diffusivities in the mixture. A knowledge of the mutual diffusivities and hence the VCCFs is essential for a complete description of mass transport in mixtures.

The mutual diffusivities for LJ [11–16] and ionic mixtures [17] in the bulk have been obtained from molecular dynamics simulations. Most of the studies of binary LJ mixtures confirm that it is essential for the mixture to be highly asymmetric to show any significant contribution from the VCCFs to mutual diffusion. Studies of LJ mixtures with varying $\mu = \sigma_{22}/\sigma_{11}$ and $\nu = \epsilon_{22}/\epsilon_{11}$ show a contribution from the distinct diffusion to mutual diffusion over a certain range of μ and ν [12]. The ratio of mutual diffusivity to the mixture self-diffusivity, $R = \mathcal{D}_{11}/\mathcal{D}_s$, is greater than unity when $\mu = 1.0$ and ν is varied. When $\nu = 1.0$ and μ is varied, R does not deviate significantly from unity [12]. Non-Lorentz-Berthelot mixtures have been investigated for the existence of mutual diffusion [13]. When the ratio $\epsilon_{12}/\epsilon_{11}$ is greater than 1.0 and $\sigma_{12}/\sigma_{11} = 1.0$, the distinct diffusion is negative ($R < 1$) and retards mutual diffusion. This suggests that the mixture is associative in nature. On the contrary, when $\epsilon_{12}/\epsilon_{11}$ is less than 1.0, the distinct diffusion is positive ($R > 1$), thereby enhancing the mutual diffusivity. This is indicative of a demixing or dissociative tendency in the mixture. As opposed to LJ mixtures, ionic mixtures show appreciable cross correlations [18]. Here the mutual diffusion is generally retarded due to the long-range attraction between the unlike ions. Studies on Ar-Kr mixtures show that, although individual VCCFs are nonzero, there is little contribution from distinct diffusion to the mutual diffusion [16]. Thus, an Ar-Kr mixture behaves like an ideal mixture from this point of view.

Molecular dynamics simulations have been extensively used to obtain self-diffusivities of fluids confined in zeolites [19–22]. In recent times, there have been a few studies of mixtures confined to the zeolitic pores by MD as well as experimental methods [23,24]. Self-diffusion studies by MD and pulse field gradient NMR of a mixture of methane and xenon in silicalite revealed that the self-diffusivity of methane is strongly influenced by the presence of xenon [23]. A mixture of CF_4 and methane in silicalite using the same methods also reports the self-diffusivities of CF_4 and methane [24]. Even though earlier studies on Ar-Kr mixtures in the bulk [16,25] suggest that the contribution from the distinct diffusivity to the mutual diffusivity is small, it is not clear how such a mixture would behave under confinement. To our knowledge the only study that computed mutual diffusivities in confined geometries using equilibrium MD simulations is the recent one by Sanborn and Snurr [26]. In this study, time correlation functions were used to obtain the Onsager coefficients and mutual diffusivities for binary mixtures of CF_4 and alkanes in the zeolite faujasite. In all cases the distinct diffusivity was found to have a positive contribution to the overall diffusivity.

The present study computes the distinct diffusivity in confined fluids. We have chosen Ar-Kr (guest) mixture confined to zeolite Y (host) since this mixture has recently been extensively studied in the bulk by Zhou and Miller [16]. In Sec. II, we briefly discuss the relevant theory. Section VI reveals some of the difficulties encountered while computing cross correlations in confined fluids by investigating a single component fluid in the zeolite NaY. The question of the existence of the distinct diffusion coefficient as normally interpreted and the need for use of appropriate reference frames is emphasized. Errors associated with the calculation of the VACF and VCCF in confined systems are discussed and we present an efficient computation scheme for evaluating the VCCF. This is employed in the study of Ar-Kr mixtures, the results of which are presented in Sec. VI. The reasons for the observed trends in the distinct diffusivity for confined mixtures of Ar and Kr are discussed.

II. THEORY

In an n -component mixture the phenomenological equations that relate the mass flux of the i th species to the gradients in mass fractions (c_k) are

$$\mathbf{J}_i = -\rho \sum_{k=1}^{n-1} D_{ik} \nabla c_k, \quad (3)$$

where $\rho = \sum_{i=1}^n \rho_i$, ρ_i is the mass density of species i , and the D_{ik} 's are the mutual or chemical diffusivities. The flux of species i in a barycentric reference frame defined with respect to the center of mass (COM) velocity \mathbf{v}^M is

$$\mathbf{J}_i = \rho_i (\bar{\mathbf{v}}_i - \mathbf{v}^M), \quad (4)$$

where $\bar{\mathbf{v}}_i$ is the average velocity of the i th species and $\mathbf{v}^M = \sum_i c_i \bar{\mathbf{v}}_i$, where c_i is the mass fraction. Hence, the fluxes satisfy

$$\sum_{i=1}^n \mathbf{J}_i = \mathbf{0}. \quad (5)$$

In a binary mixture the only independent mutual diffusivity sufficient to specify the fluxes in the mixture is D_{11} [27].

Within the framework of equilibrium statistical mechanics, the appropriate Green-Kubo relations for the mutual diffusivity in a binary mixture consisting of N_1 particles of species 1 and N_2 particles of species 2 is

$$D_{11} = \frac{Q}{3N x_1 x_2} \int_0^\infty \langle \mathbf{j}(t+\tau) \cdot \mathbf{j}(t) \rangle dt, \quad (6)$$

where $N = N_1 + N_2$ is the total number of particles, x_1 and x_2 are the mole fractions of species 1 and 2, respectively, and the relative velocity vector

$$\mathbf{j}(t) = x_2 \sum_{i=1}^{N_1} \mathbf{v}_i - x_1 \sum_{j=1}^{N_2} \mathbf{v}_j, \quad (7)$$

where \mathbf{v}_i is the velocity of particle i . In Eq. (6) the thermodynamic factor

$$Q = [1 + x_1 x_2 \rho (\Gamma_{11} + \Gamma_{22} - 2\Gamma_{12})]^{-1}, \quad (8)$$

where Γ_{ij} is related to the radial distribution function g_{ij} by

$$\Gamma_{ij} = 4\pi \int_0^\infty r^2 [g_{ij}(r) - 1] dr. \quad (9)$$

For ideal binary mixtures, Γ_{ij} are nearly identical and $Q = 1$. Substituting Eq. (7) into Eq. (6), the expression for the mutual diffusivity reduces to

$$D_{11} = Q \left(x_2 D_1 + x_1 D_2 + x_1 x_2 \left[\frac{f_{11}}{x_1^2} + \frac{f_{22}}{x_2^2} - 2 \frac{f_{12}}{x_1 x_2} \right] \right). \quad (10)$$

The above expression for the mutual diffusivity can be grouped into two main contributions:

$$D_s = Q(x_2 D_1 + x_1 D_2), \quad (11)$$

which depends on the self-diffusivities, given by

$$D_i = \frac{1}{3N} \sum_{j=1}^N \int_0^\infty \langle \mathbf{v}_j(t+\tau) \cdot \mathbf{v}_j(t) \rangle dt, \quad i=1,2, \quad (12)$$

where the integral on the right-hand side is the VACF. The distinct diffusion

$$D_d = Q \left(x_1 x_2 \left[\frac{f_{11}}{x_1^2} + \frac{f_{22}}{x_2^2} - 2 \frac{f_{12}}{x_1 x_2} \right] \right), \quad (13)$$

where

$$f_{11} = \frac{1}{3N} \sum_{i=1}^{N_1} \sum_{j \neq i}^{N_1} \int_0^\infty \langle \mathbf{v}_i(t+\tau) \cdot \mathbf{v}_j(t) \rangle dt, \quad (14a)$$

$$f_{22} = \frac{1}{3N} \sum_{i=1}^{N_2} \sum_{j \neq i}^{N_2} \int_0^\infty \langle \mathbf{v}_i(t+\tau) \cdot \mathbf{v}_j(t) \rangle dt, \quad (14b)$$

and

$$f_{12} = \frac{1}{3N} \sum_{i=1}^{N_1} \sum_{j=1}^{N_2} \int_0^\infty \langle \mathbf{v}_i(t+\tau) \cdot \mathbf{v}_j(t) \rangle dt \quad (14c)$$

are the various VCCFs and $D_{11} = D_s + D_d$.

In the Darken model for the mutual diffusivity, contributions from D_d are assumed to be negligible and $D_{11} = D_s$. This is applicable for dilute [28] binary mixtures of rare gases where the thermodynamic factor is nearly unity. The contributions from the distinct diffusion D_d can increase or decrease the overall mutual diffusivity. In order to evaluate this effect we define a ratio

$$R = \frac{D_{11}}{D_s}. \quad (15)$$

$R > 1$ indicates that D_d enhances the mutual diffusivity and $R < 1$ indicates a retarding effect. The diffusivities in Eq. (15) and later reported in this work are

$$\mathcal{D}_s = D_s / Q \quad \text{and} \quad \mathcal{D}_d = D_d / Q. \quad (16)$$

III. STRUCTURE OF ZEOLITE NaY

The zeolite NaY chosen for the study is the sodium form with Si/Al = 3.0 and unit cell composition $\text{Na}_{48}\text{Si}_{144}\text{Al}_{48}\text{O}_{384}$ [29]. Each unit cell has eight large cages known as super-cages or α -cages of approximately 11.8 Å diameter interconnected with each other in a tetrahedral manner through 12-membered rings of about 7.8 Å free diameter. The voids form a three-dimensional network through which sorbates can diffuse. Figure 1 shows two α cages of zeolite NaY and eight α cages that are present in one crystallographic unit cell.

IV. INTERACTION POTENTIAL

Guest-guest and guest-host interactions were modeled in terms of the (6-12) LJ potential. The latter was confined to interactions between the oxygen and sodium atoms of the zeolite framework. Short-range interactions between the guest and Si/Al are not considered since the close approach of the guest toward Si or Al is prevented by the bulkier oxygen atoms. The zeolite framework itself is assumed to be rigid and is not included in the molecular dynamics integration, unless stated otherwise. In the rigid framework simulations, the total potential energy is the sum of the guest-guest and the guest-host interactions. The potential parameters for unlike particles were obtained using Lorentz-Berthelot combination rules. The LJ parameters for the guest and host atoms are given in Table I:

$$U_{tot}^{LJ} = \sum_i^N \sum_{j < i}^N U_{gg}(r_{ij}) + \sum_i^N \sum_j^{N_z} U_{gh}(r_{ij}), \quad (17)$$

$$U(r_{ij}) = 4 \epsilon [(\sigma/r_{ij})^{12} - (\sigma/r_{ij})^6], \quad (18)$$

where N and N_z are the number of guest and zeolite atoms, respectively.

When the zeolite cage was not assumed to be rigid, the framework atoms were allowed to move using a harmonic potential [30]

$$U = \frac{1}{2} k (r - r_0)^2, \quad (19)$$

where the values of the spring constant k and equilibrium bond length r_0 are given in Ref. [30].

V. SIMULATION DETAILS

All simulations have been carried out in the microcanonical (N - V - E) ensemble with cubic periodic boundary conditions [31]. The number of guest particles N is 512 at a concentration of 8 atoms/ α cage. A neutron diffraction study by

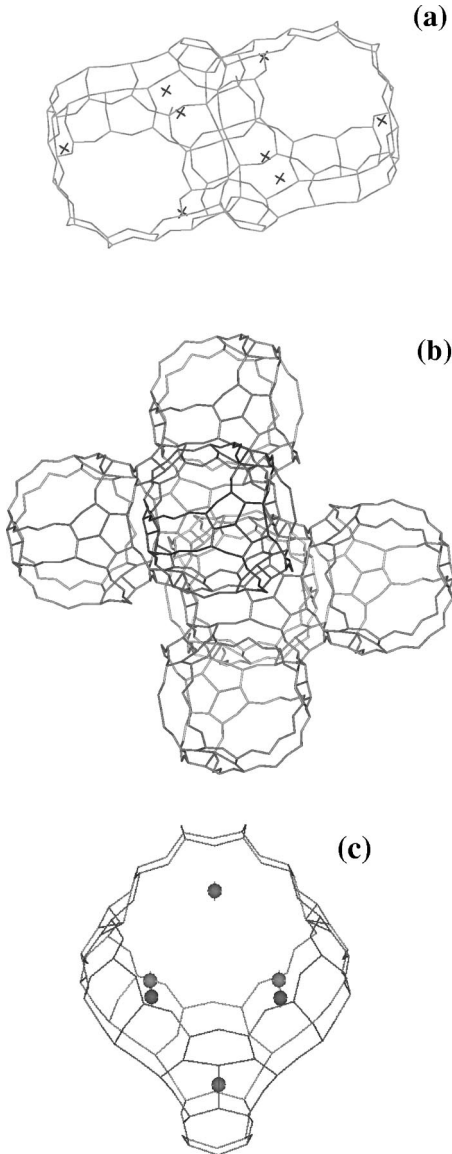


FIG. 1. Structure of the zeolite NaY. (a) Two α cages of zeolite NaY where the crosses represent the extra framework cations (Na). (b) Eight α cages of zeolite NaY connected tetrahedrally to each other via 12-ring windows. The smaller cages such as the sodalite are not shown for clarity. Guest molecules diffuse through the α cages since the smaller sodalite cages are inaccessible. (c) A single α cage showing the six physisorption sites of Ar/Kr.

Fitch *et al.* indicated that NaY crystallizes in the $Fd\bar{3}m$ space group with the lattice parameter $a = 24.85$ Å. In the present study, we have employed $2 \times 2 \times 2$ unit cells leading to a simulation cell with an edge length of 49.70 Å. A potential cutoff of $r_c = 12$ Å has been employed for guest-guest and guest-host interactions. Each α cage has eight guest atoms, which corresponds to a number density of 0.0124 Å⁻³. The cage volume was calculated by considering that the cage is a spherical cavity of radius 5.36 Å. In single component studies all eight atoms were Ar, and in mixture studies there were four each of argon and krypton.

Each MD run was 300 ps long for single component studies and 1.5 ns for mixture studies. Typically eight such runs

TABLE I. Lennard-Jones parameters.

	σ (Å)	ϵ (kJ/mol)
Ar-Ar	3.405	0.998
Kr-Kr	3.633	1.388
O-O	2.545	1.289
Na-Na	3.369	0.0392

were carried out to obtain more accurate estimates. Equations of motion were integrated with the velocity Verlet algorithm [31]. The equilibration period was 300 and 500 ps for single component and mixture studies, respectively. An integration time of 10 fs has been found to yield adequate energy conservation. Positions and velocities were stored every 20 fs for calculating properties of interest.

VI. RESULTS AND DISCUSSION

Calculations of time correlation functions (TCFs) and, in particular, the VCCFs of confined fluids provide certain additional difficulties not generally encountered in bulk fluids. In order to understand these, we first report here the single component studies of Ar in the zeolite NaY.

A. Single component studies

The VACFs and VCCFs were computed for Ar confined to the pores of the zeolite NaY at a loading of 8 atoms/ α cage at 300 K. The VCCFs are shown in Fig. 2(a) for 40 ps. Large amplitude oscillations persist. Earlier MD simulations by Balucani and co-workers and others [8,9] on bulk fluids found that the decay of VCCFs occurs in 1–2 ps. In order to understand these undecaying oscillations, we computed the velocity of the COM of the system:

$$\mathbf{v}^M = \frac{1}{N} \sum_{i=1}^N \mathbf{v}_i. \quad (20)$$

We computed the VACF of the COM velocities:

$$C^M(t) = \langle \mathbf{v}^M(\tau+t) \cdot \mathbf{v}^M(\tau) \rangle_{\tau}, \quad (21)$$

which is shown in Fig. 2(b) for 10 ps. We found that the total momentum of the system was not conserved and this is evident from the presence of oscillations in the COM VACF. This is an inherent problem in confined systems. In the present case, the zeolite, which is treated as a rigid framework, provides an external force. We also carried out simulations in a flexible framework by including the zeolite atoms in the MD integration. A harmonic potential proposed by Demontis and co-workers [30] was used for integrating the zeolite atoms [see Eq. (19)]. The oscillations in the VCCFs are shown as an inset to Fig. 2(a). Note that the oscillations still persist with slightly lower amplitudes. When the MD integration includes both the guest and zeolite atoms, the total momentum of the system consisting of guest and zeolite atoms is conserved. However, the total momentum of the guest subsystem is still not conserved.

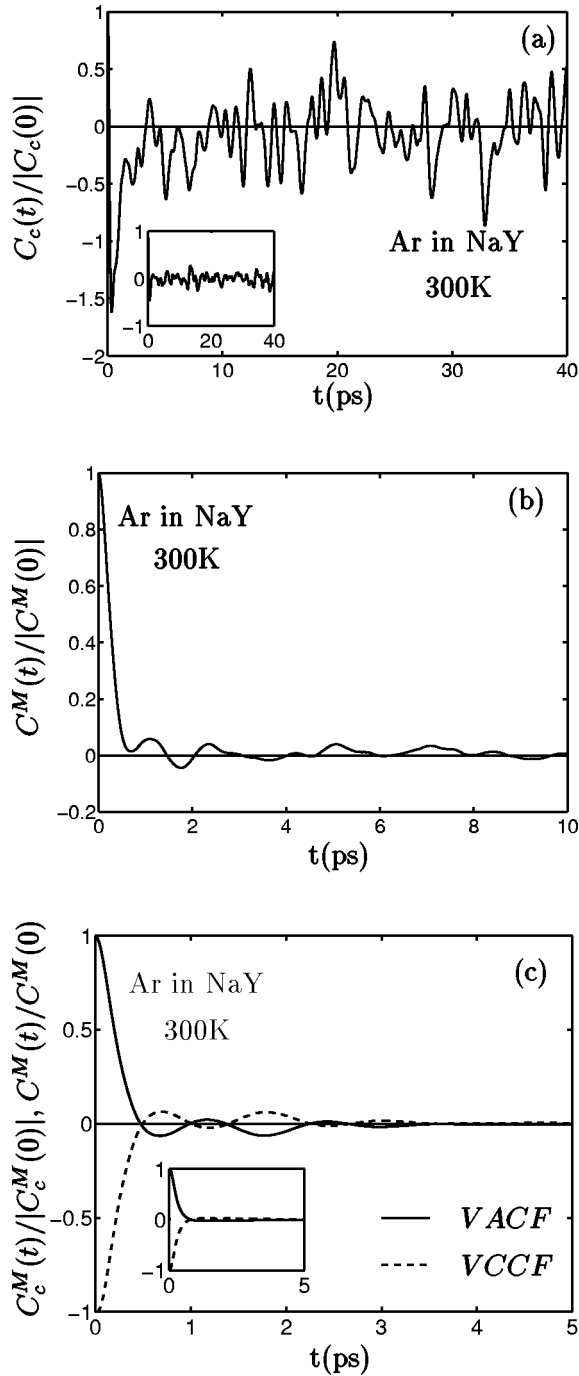


FIG. 2. Velocity auto- and cross correlation functions of single component argon in NaY at 300 K. (a) $C_c(t)/|C_c(0)|$ without COM corrections with zeolite atoms held rigid. $C_c(t)/|C_c(0)|$ without COM corrections for a flexible framework is shown in the inset. (b) COM autocorrelation function. (c) The auto- and cross correlations in the barycentric reference frame in the rigid framework approximation; inset shows auto- and cross correlations for a flexible framework.

The presence of large amplitude, long-time oscillations raises doubts about the very existence of the integrals [Eq. (14)] that are required to obtain D_{11} or D_d . In relation to this problem, Raineri and Friedman [32,33] have discussed the importance of reference frames while calculating VCCFs in

particular and TCFs in general. The diffusion fluxes of various components in a binary or multicomponent mixture and the thermodynamic forces are related via the mutual diffusivity. The diffusion fluxes are usually defined relative to a suitable reference frame. Therefore, the chemical or mutual diffusivities are known to be dependent on the reference frame used. In the microscopic equations relating the chemical diffusivity to the self-diffusivity and the distinct diffusivity, we know that the self-diffusion coefficients are independent of the reference frame used. The reference frame dependence of the mutual diffusivity therefore arises solely due to the reference dependence of the distinct diffusivity. In order to guarantee the existence of the TCFs, the dynamical variables used in deriving the TCFs should be orthogonal to the constants of motion relevant to the problem at hand. Here the velocities of the atoms should be orthogonal to the total linear momentum of the system. There are several internal reference frames in which this can be achieved. We have chosen the barycentric reference frame, in which the reference frame velocity is defined as

$$\mathbf{v}^M = \frac{\sum_{i=1}^N m_i \mathbf{v}_i}{\sum_{i=1}^N m_i}. \quad (22)$$

In order to evaluate quantities in the barycentric reference frame we transform the velocities $\mathbf{v}_i(t)$ using

$$\mathbf{v}_i^M(t) = \mathbf{v}_i(t) - \mathbf{v}^M(t), \quad (23)$$

where $\mathbf{v}_i^M(t)$ are the velocities in the barycentric reference frame. For single component fluids, Eq. (22) reduces to Eq. (20). Time correlation functions and diffusivities computed in the barycentric reference frame are expected to be well behaved. Figure 2(c) illustrates the VCCF computed in the barycentric reference frame. When compared with the VCCF computed using the original trajectories [Fig. 2(a)], without attention to the reference frame [26], we find that the long-time oscillations and the large positive regions at initial times are absent. Since all properties reported in this paper are computed in the barycentric reference frame, the superscript M will be dropped henceforth.

Although the appropriate choice of reference frames is crucial while evaluating cross correlations, the influence of the COM motion on the VACF is negligible and is usually ignored [32] while computing self-diffusivities of confined fluids. We analyzed this by relating the VCCF and VACF computed in the barycentric reference frame to those computed using the original trajectories. This is analyzed in Appendixes A and B, where it is shown that the contributions to the VCCF from the COM VACF are of the same order of magnitude ($1/N$) as those arising from the cross correlations. However, the contributions from the COM VACF toward the VACF is $O(1/N^2)$ and hence can be neglected. For the system size used in this study, VACFs computed using $\mathbf{v}_i^M(t)$ and $\mathbf{v}_i(t)$ were identical. The analysis in Appendix B also

illustrates that the property $VCCF = -VACF$ [32] is recovered in the barycentric reference frame as observed in Fig. 2(c).

We also provide in Appendix C an efficient method for the computation of VCCFs, which is a simplification of methods that are currently in use. This reduces an $O(N^2)$ problem to $O(N)$ in the case of the calculation of VCCFs between like species [$C_c^{11}(t)$ and $C_c^{22}(t)$] and $O(1)$ in the case of VCCFs between unlike species [$C_c^{12}(t)$]. Once the VACFs have been computed, all the VCCFs can be computed with an $O(1)$ algorithm. As a result, the computational effort required is drastically reduced, enabling the computation of the VCCFs to be performed on relatively small computing platforms. The expressions listed in Appendix C also bring out the fact that the VCCFs are collective properties.

B. Binary mixture studies

To begin, we note that the Ar-Kr mixture shows no contribution from distinct diffusivities \mathcal{D}_d to the mutual diffusion coefficient \mathcal{D}_{11} in the bulk [16]. Velocity auto- and cross correlation functions for the Ar-Kr mixture confined to a NaY zeolite were computed at 200 and 600 K at a loading of eight atoms per α cage and are shown in Fig. 3. For clarity the VCCFs at 200 K have been shifted by 0.2 units and the negative regions at short times have not been shown. The VCCFs shown in Fig. 3 were obtained by averaging over eight runs of 1.5 ns each. The inset in Fig. 3(b) shows the VCCF obtained from a single 1.5 ns run. Large fluctuations are evident, which are considerably reduced on averaging over the eight runs. Further, it is seen that the VCCFs show significant oscillations up to 120 ps, with greater oscillations for Ar-Ar VCCF [Fig. 3(b)] due to the lower mass of Ar, when compared with the Ar-Kr or Kr-Kr VCCF. The magnitudes of fluctuations at both 200 and 600 K are comparable. Note that, although oscillations persist, the magnitude of oscillations is significantly lower than those seen in Fig. 2(a). The reason for these oscillations is twofold. As pointed out by Zhou and Miller and shown in Appendix C, VCCFs are collective quantities and therefore show larger fluctuations in comparison to the VACFs, which are averaged over N particles of the system. The accuracy with which the VCCFs can be obtained is therefore significantly lower. Secondly, unlike in the bulk, the potential energy surface within the zeolite is highly undulating with deep minima and maxima. These lead to larger errors even in the calculation of VACFs as was shown recently [34].

Figures 4(a) and 4(b) show f_{ij} [Eq. (14)] for 200 and 600 K. These curves have been averaged over eight runs after carrying out integrations on the individual VCCFs. The integral converges to a well defined value by about 20 ps. Beyond 20 ps, the curves fluctuate around a mean value. While estimating the integrals in Eq. (14), we discarded values below 20 ps. Further, this suggests that there may be low frequency modes that have a relaxation time up to around 20 ps. Such modes are clearly absent in bulk [16], where all three f_{ij} typically decay within 2ps. Usually, f_{12} lies between those of f_{11} and f_{22} as seen in Fig. 4(b) at 600 K. In Fig. 5(a), which shows the behavior at 200 K, it is seen that this is not

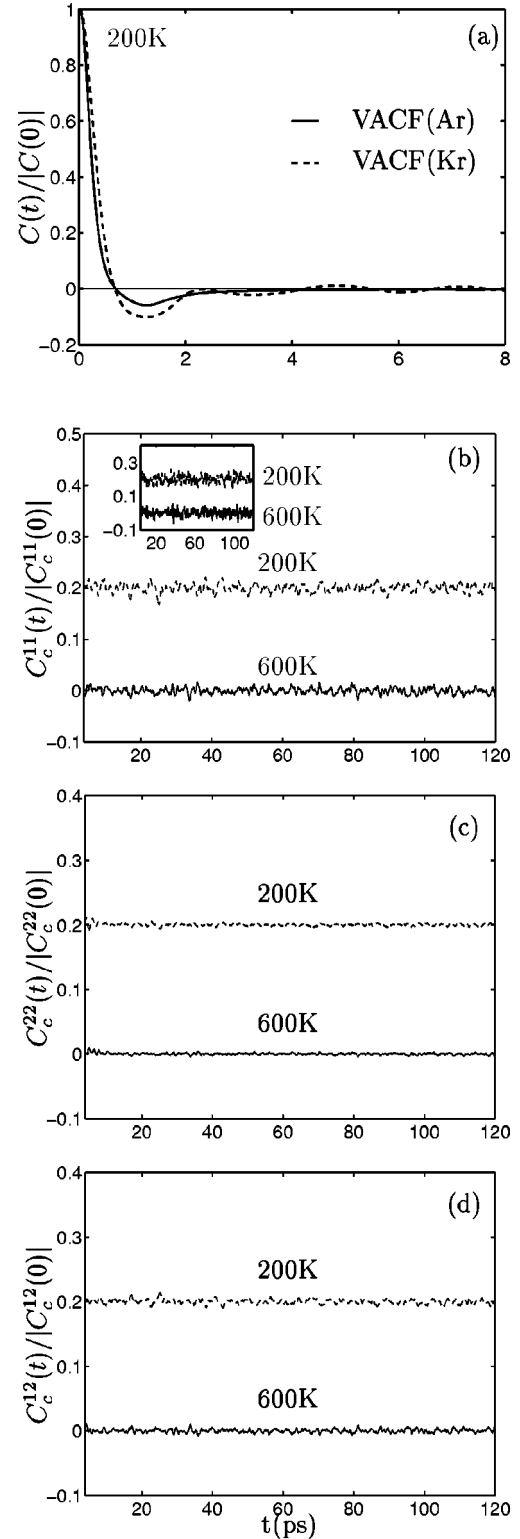


FIG. 3. (a) Normalized velocity autocorrelation function for argon and krypton in NaY at 200 K. Normalized cross correlation functions averaged over eight runs each of 1.5 ns are shown in (b)–(d) at 200 (dashed) and 600 K (continuous). (b) $C_c^{11}(t)/|C_c^{11}(0)|$. Inset shows VCCF for Ar calculated using a single run. (c) $C_c^{22}(t)/|C_c^{22}(0)|$. (d) $C_c^{12}(t)/|C_c^{12}(0)|$. Label 1 represents argon and label 2 represents krypton. The cross correlations at 200 K are shifted by 0.2 units.

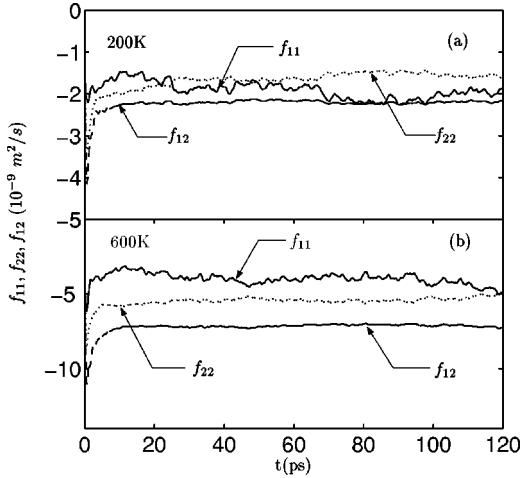


FIG. 4. Running integrals of cross correlation functions averaged over eight runs (a) at 200 K and (b) at 600 K.

the case: f_{12} has a higher value than f_{11} and f_{22} . Later, we show that this leads to a negative value for \mathcal{D}_d .

Figures 5(a) and 5(b) show \mathcal{D}_d [Eq. (13)] calculated from individual runs (dashed lines) and \mathcal{D}_d averaged over eight runs (solid lines) at 200 and 600 K, respectively. Even after averaging over eight runs, it is seen that there are slight variations in \mathcal{D}_d with time. In order to assess the error asso-

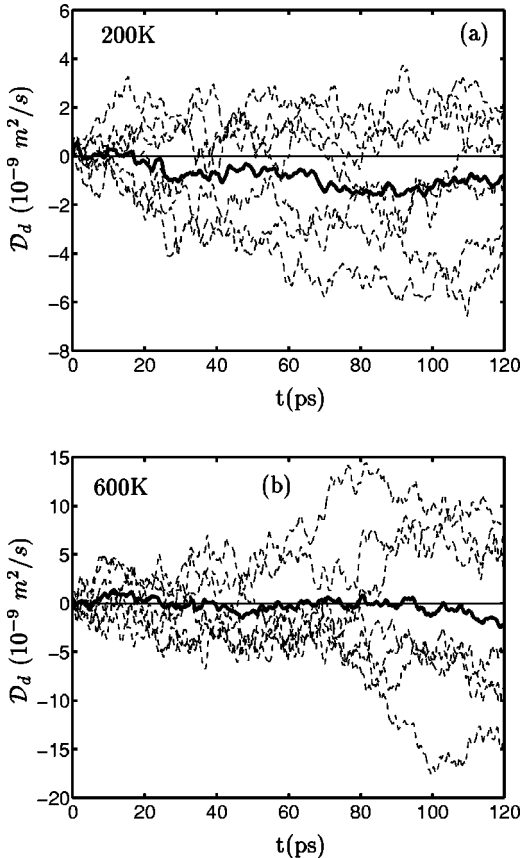


FIG. 5. Distinct diffusion \mathcal{D}_d from individual runs (dashed lines) and \mathcal{D}_d (solid line) averaged over eight simulation runs at (a) 200 K and (b) 600 K.

ciated with the computed values of \mathcal{D}_d , we computed its mean and variance. The mean value of \mathcal{D}_d for each of the eight runs, $(\bar{\mathcal{D}}_d)_i$, $i=1,2,\dots,8$, was calculated by averaging over all time steps between 20 and 120 ps. The variance for $\bar{\mathcal{D}}_d$ was obtained using [35]

$$s^2 = \frac{p}{m-1} \sum_{i=1}^{m-1} [(\bar{\mathcal{D}}_d)_i - \bar{\mathcal{D}}_d]^2, \quad (24)$$

where $\bar{\mathcal{D}}_d$ was obtained from the VCCF by averaging over all the eight runs [shown in Figs. 5(a) and 5(b) as solid lines] again using data in the 20–120 ps range. Here $m=8$ and $p=1.5$ ns. The variance of $\bar{\mathcal{D}}_d$ is given by $\sigma_D^2 = s^2/L$, where $L=mp$. The value of \mathcal{D}_d averaged over the eight runs and the standard deviations is shown in Table II. As previously pointed out, the errors in the \mathcal{D}_d are quite large. In the case of 600 K, the errors are comparable to the magnitude of \mathcal{D}_d .

Figure 6 shows the time-dependent self-diffusivities $D_1(t)$, $D_2(t)$ obtained by integrating the VACFs for argon and krypton along with \mathcal{D}_s [Eq. (11)]. These converge within 5–8 ps as compared with 20 ps found for the VCCFs. Due to the small fluctuation in the VACFs, \mathcal{D}_s was obtained from a single 1.5 ns run. Table II lists the values of D_1 , D_2 , the self-diffusivities of argon and krypton, respectively, \mathcal{D}_s , and \mathcal{D}_d for 200 and 600 K. At both 200 and 600 K, \mathcal{D}_d values are negative, with the value at 200 K significantly more negative than the value at 600 K. The ratio $R = \mathcal{D}_{11}/\mathcal{D}_s$ given in Table II is indicative of the relative contribution of the distinct diffusion to the mutual diffusivity. $R < 1$ signifies negative contributions and $R > 1$ signifies positive contributions from the distinct diffusivity to the mutual diffusivity. The value of \mathcal{D}_d at 200 K is significant with $\mathcal{D}_{11}/\mathcal{D}_s = 0.769$, indicating that the ratio of the distinct diffusivity to self-diffusivity ($1 - R$) is about 23%. At 600 K a value of $\mathcal{D}_{11}/\mathcal{D}_s = 0.966$ implies that the distinct diffusion, although weak, has a small negative contribution to the overall mutual diffusivity.

Earlier studies on Lorentz-Berthelot mixtures found only a positive contribution from \mathcal{D}_d ($R > 1$) to mutual diffusion [12]. For non-Lorentz-Berthelot mixtures, R values as low as 0.827 have been reported [13]. The only systems to show a negative contribution from \mathcal{D}_d other than non-Lorentz-Berthelot mixtures are ionic systems. The value of R observed here for confined Ar-Kr mixtures at 200 K is significantly smaller than unity, even though they behave as ideal mixtures in the bulk with zero contribution from \mathcal{D}_d [16]. These results suggest that confinement or the presence of an external field affects not only the self-diffusivity known, but also the distinct diffusivity.

TABLE II. The self-diffusion coefficients (D_1 and D_2) of Ar and Kr, \mathcal{D}_s and distinct diffusion coefficient \mathcal{D}_d , and variance in distinct diffusion coefficient in 10^{-8} m²/s.

T (K)	D_1	D_2	\mathcal{D}_s	\mathcal{D}_d	σ_D	$R = \mathcal{D}_{11}/\mathcal{D}_s$
200	0.536	0.3042	0.4201	-0.0969	0.0158	0.7693
600	1.447	0.911	1.179	-0.0405	0.0407	0.966

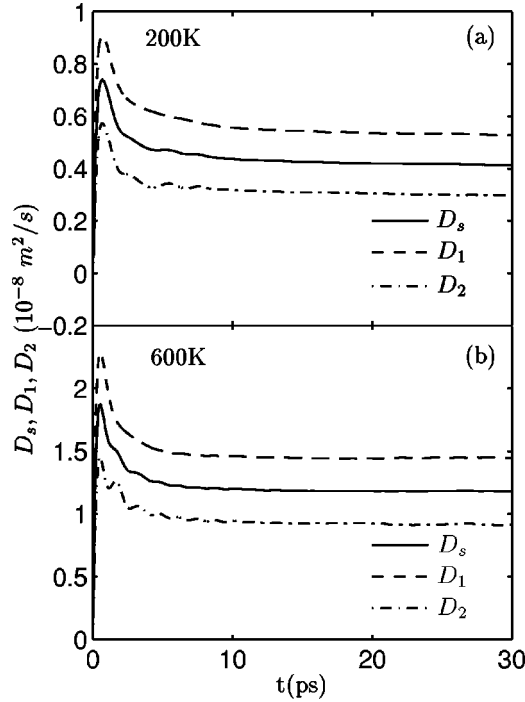


FIG. 6. Self-diffusivities D_1 , D_2 , and D_s at (a) 200 and (b) 600 K. Labels 1 and 2 represent Ar and Kr, respectively.

Figures 7(a) and 7(b) display plots of the radial distribution functions between Ar-Ar (g_{11}), Ar-Kr (g_{12}), and Kr-Kr (g_{22}). The radial distribution functions show no noticeable deviation from normal bulk liquid structures. g_{12} lies between g_{11} and g_{22} as one would expect for a Lorentz-Berthelot mixture. The increased negative correlation in \mathcal{D}_d seems to leave no signature in the equilibrium structure of the fluid. In contrast, our recent studies on slit pores show that negative values in \mathcal{D}_d are associated with increased intensity in $g_{12}(r)$. Since distinct diffusivity is a TCF, characteristics of the f_{ij} need not necessarily be reflected in the $g(r)$. Alternatively, the dynamic structure factor may provide greater insight into the trends observed in the f_{ij} reported here. However, since \mathcal{D}_d is significant at 200 K and small at 600 K we looked at typical trajectories of Ar and Kr in the zeolite at these temperatures. Figure 8 shows the single particle trajectories of krypton and argon at 200 and 600 K. At 600 K both Ar and Kr spend hardly any time at the physisorption site, as is evident from the highly delocalized trajectory. In contrast, at 200 K the guest particles spend a significant amount of time in the physisorption sites. There are six such physisorption sites in each cage as illustrated in Fig. 1(c).

The relative magnitudes of f_{ij} (Fig. 4) determine whether the distinct diffusion is negative or positive. At 200 K [Fig. 4(a)] the relative behavior in f_{ij} below 20 ps is typical of the trend observed in an ideal mixture with f_{12} lying between f_{11} and f_{22} . However, a crossover between f_{11} and f_{12} is seen at around 30 ps [Fig. 4(a)]: the magnitude of f_{11} increases while that of f_{12} decreases. In addition, we notice a change in f_{11} and f_{12} around 70 ps. The fact that the magnitude of f_{12} has decreased relative to f_{11} and f_{22} [Fig. 4(a)] is responsible

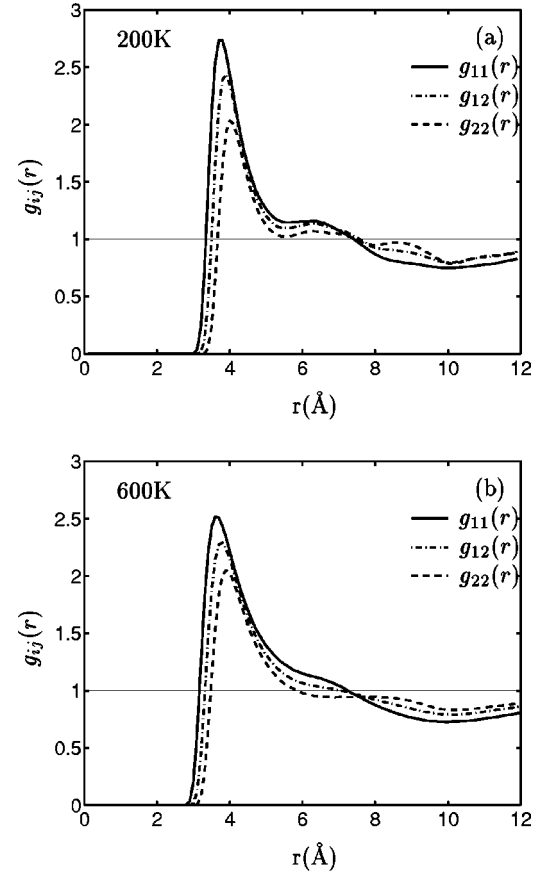


FIG. 7. Radial distribution functions (a) at 200 K and (b) at 600 K. Label 1 represents Ar and label 2 represents Kr.

for the negative value of \mathcal{D}_d (Table II). These changes that occur at large time scales could arise from the large residence times of the guest atoms in the physisorption sites which alter the dynamic correlation between particles. At 600 K [Fig. 4(b)] f_{12} lies between f_{11} and f_{22} for the entire duration of 120 ps.

From Eq. (10) it is clear that the mixture is dissociative if $|f_{11} + f_{22}| < |2f_{12}|$ and is associative if $|f_{11} + f_{22}| > |2f_{12}|$ (Table III). This leads to $\mathcal{D}_d > 1$ for dissociative mixtures and $\mathcal{D}_d < 1$ for associative mixtures. At 600 K, the mixture does not show any appreciable associative tendency and the contribution from the cross correlations to the mutual diffusion is small. Although the net contribution from the cross correlations ($f_{11} + f_{22} - 2f_{12}$) to the distinct diffusion is nearly zero, strong individual cross correlations (f_{ij}) are present as seen in Table III. This is similar to what was found in the bulk mixture [16].

The Darken and common force models are two models that attempt to predict the mutual diffusivities. The Darken model assumes the distinct diffusivity to be zero and in the case of the common force model the distinct diffusivity is always negative. The common force model therefore appears more appropriate to the present problem. The values of mutual diffusivity obtained from these two models and MD are listed in Table IV. It is seen that at 200 K both models predict a value of mutual diffusivity that is higher than that obtained from MD simulations. At 200 K, when particles spend a considerable fraction of time at the adsorption sites,

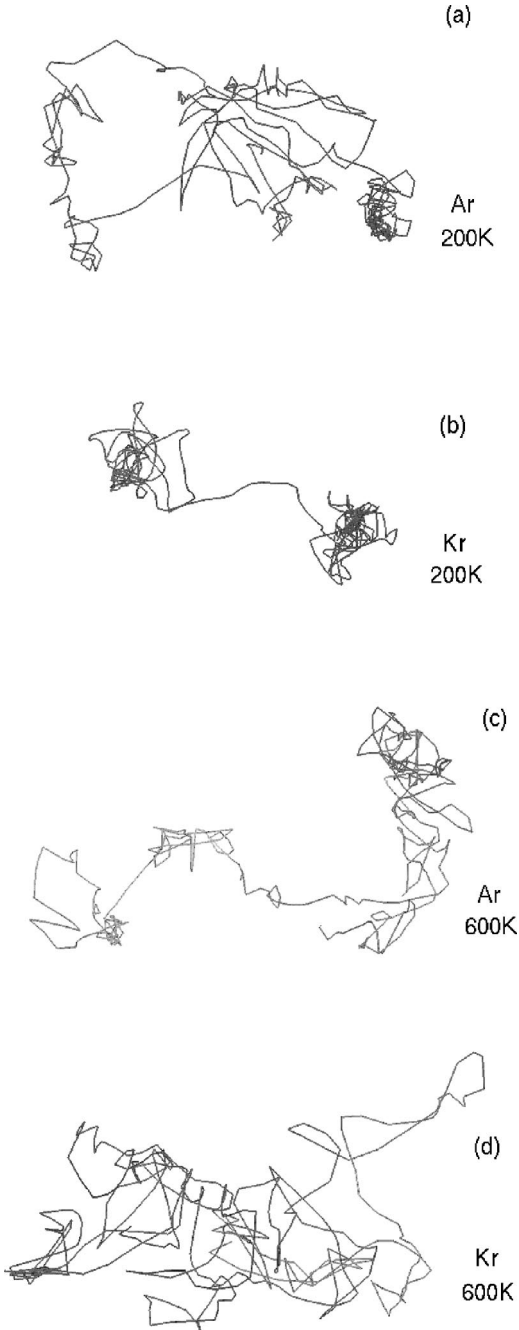


FIG. 8. The trajectories of a single representative particle in the binary NaY-Ar-Kr system. (a) Trajectory of Ar at 200 K, (b) trajectory of Kr at 200 K, (c) trajectory of Ar at 600 K, and (d) trajectory of Kr at 600 K.

resulting in noticeable cross correlations ($R < 1$), the common force model provides a closer estimate of the mutual diffusivity. At 600 K, where \mathcal{D}_d is small, both models predict values that are close to the MD value.

Our results and discussion are based on the ratios of $\mathcal{D}_{11}/\mathcal{D}_s$. In order to use the mutual diffusivity in evaluating the fluxes of various species in the mixture, a knowledge of the thermodynamic factor Q is necessary. The calculation of the thermodynamic factor Q requires a knowledge of the radial distribution functions $g(r)$. Unlike the situation in a bulk

TABLE III. Integrals of the VCCFs in 10^{-8} m²/s.

$T(K)$	f_{11}	f_{22}	f_{12}	$ f_{11}+f_{22} $	$ 2f_{12} $
200	-0.1956	-0.2197	-0.15924	0.4153	0.31848
600	-0.4042	-0.7128	-0.5383	1.117	1.0766

fluid, where $g(r)$ converges to unity within $(2-3)\sigma$, under confinement $g(r)$ shows peaks beyond 2σ or 3σ and therefore the integrals Γ_{ij} in Eq. (8) do not converge. The presence of structure in Ar-Ar (or Ar-Kr or Kr-Kr) radial distribution functions at large r is due to the crystalline structure of the host. Simulations of larger systems are required to estimate Q .

VII. CONCLUSION

The Ar-Kr mixture, which shows zero distinct diffusivity in the bulk, exhibits significant negative values when confined to the zeolite NaY. Earlier work by several groups found that only mixtures that have high asymmetry in the potential parameters can exhibit noticeable nonzero distinct diffusivity in bulk. In contrast, the present work shows that even mixtures with little asymmetry in their interaction potentials can show significant distinct diffusivity when confined. We attribute this to the presence of adsorption sites, which alter the dynamics and therefore the transport properties.

We also show that appropriate choice of the reference frame is important for evaluating the velocity cross correlation functions. The existence of f_{ij} is not guaranteed unless the VCCFs are calculated in the correct reference frame [32]. This dependence of the VCCF on the reference frame arises from the dependence of flux on the choice of the reference frame. Since in the bulk the total momentum is conserved, the evaluation of the VCCF from an N - V - E MD simulation ensures that the reference frame is barycentric. Under confinement the diffusing species forms only a part of the total system where the total momentum is not conserved. In such a situation, choice of the reference frame is crucial. The reference frame dependence of the VACFs and VCCFs are discussed in the Appendixes along with an efficient method for the calculation of the latter.

Zeolites are well known for their molecular sieving property. They are used extensively for separation of hydrocarbons and other mixtures. The nonzero distinct diffusivity of even ideal mixtures when confined to zeolites such as NaY

TABLE IV. The mutual diffusivity \mathcal{D}_{11} in 10^{-8} m²/s calculated from Eq. (10) compared with the values predicted using the Darken and common force models.

$T(K)$	\mathcal{D}_{11} Darken	\mathcal{D}_{11} common force	\mathcal{D}_{11}
200	0.4201	0.38812	0.323
600	1.179	1.1180	1.1385

does have implications for separation properties displayed by the zeolites for a given mixture. This study also shows that transport coefficients normally obtained from rather time-consuming nonequilibrium MD simulations may be obtained from equilibrium MD simulations. A number of factors influence the distinct diffusivity in a confined system, one of which is the geometry of the pore. We are presently investigating this aspect.

APPENDIX A: VACF

The velocity autocorrelation function for a single component system consisting of N particles,

$$C(t) = \langle \mathbf{v}(\tau) \cdot \mathbf{v}(\tau+t) \rangle_{\tau, N} \quad (\text{A1})$$

$$= \left\langle \frac{1}{N} \sum_i \mathbf{v}_i(\tau) \cdot \mathbf{v}_i(\tau+t) \right\rangle_{\tau}, \quad (\text{A2})$$

where the summation runs over N particles. The velocities in the barycentric reference frame are

$$\mathbf{v}_i^M(\tau) = \mathbf{v}_i(\tau) - \mathbf{v}^M(\tau), \quad (\text{A3})$$

where $\mathbf{v}^M(\tau)$, the velocity of the COM, is defined in Eq. (22) of the text. Substituting $\mathbf{v}_i(\tau)$ from Eq. (A3) into Eq. (A2) and simplifying,

$$C(t) = \left\langle \frac{1}{N} \sum_i \{ [\mathbf{v}_i^M(\tau) + \mathbf{v}^M(\tau)] \cdot [\mathbf{v}_i^M(\tau+t) + \mathbf{v}^M(\tau+t)] \} \right\rangle_{\tau}. \quad (\text{A4})$$

In a single-component system,

$$\begin{aligned} C(t) &= \frac{1}{N} \left\langle \sum_i \mathbf{v}_i^M(\tau) \cdot \mathbf{v}_i^M(\tau+t) \right\rangle_{\tau} \\ &+ \frac{1}{N^2} \langle \mathbf{S}^M(\tau) \cdot \mathbf{S}(\tau+t) \rangle_{\tau} \\ &+ \frac{1}{N^2} \langle \mathbf{S}(\tau) \cdot \mathbf{S}^M(\tau+t) \rangle_{\tau} \\ &+ \frac{1}{N^2} \langle \mathbf{S}(\tau) \cdot \mathbf{S}(\tau+t) \rangle_{\tau}, \end{aligned} \quad (\text{A5})$$

where

$$\mathbf{S}(\tau) = \sum_i \mathbf{v}_i(\tau)$$

and

$$\mathbf{S}^M(\tau) = \sum_i \mathbf{v}_i^M(\tau).$$

Since $\mathbf{S}^M(\tau) = \mathbf{0}$, the second and third terms in Eq. (A5) are identically zero. Hence

$$C(t) = C^M(t) + \frac{1}{N^2} \langle \mathbf{S}(\tau) \cdot \mathbf{S}(\tau+t) \rangle_{\tau}, \quad (\text{A6})$$

where

$$C^M(t) = \frac{1}{N} \left\langle \sum_i \mathbf{v}_i^M(\tau) \cdot \mathbf{v}_i^M(\tau+t) \right\rangle_{\tau}.$$

Since the last term in Eq. (A6), which is the COM autocorrelation function, scales as N^{-2} , the contributions to the VACF from the COM velocity are negligible for sufficiently large systems and $C(t) = C^M(t)$.

APPENDIX B: VCCF

The velocity cross correlation function for a single-component system consisting of N particles,

$$C_c(t) = \left\langle \frac{1}{3N} \sum_i \sum_{j \neq i} \mathbf{v}_i(\tau) \cdot \mathbf{v}_j(\tau+t) \right\rangle_{\tau}. \quad (\text{B1})$$

Substituting for $\mathbf{v}_i(\tau)$ from Eq. (A3),

$$\begin{aligned} C_c(t) &= \frac{1}{3N} \left[\left\langle \sum_i \sum_{j \neq i} \mathbf{v}_i^M(\tau) \cdot \mathbf{v}_j^M(\tau+t) \right\rangle_{\tau} \right. \\ &+ \frac{N-1}{N} \langle \mathbf{S}^M(\tau) \cdot \mathbf{S}(\tau+t) \rangle_{\tau} \\ &+ \frac{1}{N} \left\langle \sum_i \sum_{j \neq i} \mathbf{S}(\tau) \cdot \mathbf{v}_j^M(\tau+t) \right\rangle_{\tau} \\ &\left. + \frac{N-1}{N} \langle \mathbf{S}(\tau) \cdot \mathbf{S}(\tau+t) \rangle_{\tau} \right]. \end{aligned} \quad (\text{B2})$$

Since $\mathbf{S}^M(\tau) = \mathbf{0}$, the second and third terms in Eq. (B2) are identically zero and Eq. (B2) reduces to

$$\begin{aligned} C_c(t) &= C_c^M(t) + \frac{1}{3N} \langle \mathbf{S}(\tau) \cdot \mathbf{S}(\tau+t) \rangle_{\tau} \\ &- \frac{1}{3N^2} \langle \mathbf{S}(\tau) \cdot \mathbf{S}(\tau+t) \rangle_{\tau}, \end{aligned} \quad (\text{B3})$$

where the expression for $C_c^M(t)$ is similar to that in Eq. (B1), with the velocities \mathbf{v}_i replaced by \mathbf{v}_i^M . For large N , Eq. (B3) can be simplified to

$$C_c(t) = C_c^M(t) + \frac{1}{3N} \langle \mathbf{S}(\tau) \cdot \mathbf{S}(\tau+t) \rangle_{\tau}. \quad (\text{B4})$$

Equation (B4) indicates that the COM autocorrelation function is $O(N^{-1})$, which is similar to that of the VCCF. Noting that the VCCF can be rewritten as

$$C_c(t) = \frac{1}{3N} \langle \mathbf{S}(\tau) \cdot \mathbf{S}(\tau+t) \rangle_\tau - C(t), \quad (\text{B5})$$

Eq. (B4) reduces to

$$C_c^M(t) = -C(t). \quad (\text{B6})$$

This relationship is observed in Fig. 2(c) where the TCFs are computed in the barycentric reference frame. Our analysis [Eq. (B4)] also reveals that the VCCF computed with the original velocities [$C_c(t)$] without using a proper reference frame will have positive contributions at initial times as seen in Fig. 2(a).

APPENDIX C: COMPUTATION OF VCCF IN BINARY MIXTURES

In a binary mixture with N_1 particles of type 1 and N_2 particles of type 2, there are three VCCFs $C_c^{11}(t)$, $C_c^{22}(t)$, and $C_c^{12}(t)$. Consider

$$C_c^{11}(t) = \left\langle \sum_{i=1}^{N_1} \sum_{j \neq i}^{N_1} \mathbf{v}_i(\tau) \cdot \mathbf{v}_j(\tau+t) \right\rangle_\tau, \quad (\text{C1})$$

where the factor $1/(3N)$ has been omitted for convenience. Computation of Eq. (C1) requires evaluation of $O(N^2)$ terms. We rewrite Eq. (C1) as

$$C_c^{11}(t) = \left\langle \sum_{i=1}^{N_1} \mathbf{v}_i(\tau) \cdot \sum_{j \neq i}^{N_1} \mathbf{v}_j(\tau+t) \right\rangle_\tau \quad (\text{C2})$$

$$= \left\langle \sum_{i=1}^{N_1} \mathbf{v}_i(\tau) \cdot \left[\sum_{j=1}^{N_1} \mathbf{v}_j(\tau+t) - \mathbf{v}_i(\tau+t) \right] \right\rangle_\tau \quad (\text{C3})$$

$$= \langle \mathbf{S}_1(\tau) \cdot \mathbf{S}_1(\tau+t) \rangle - C^1(t), \quad (\text{C4})$$

where $\mathbf{S}_1(\tau) = \sum_{i=1}^{N_1} \mathbf{v}_i(\tau)$ and $C^i(t)$ is the autocorrelation function [Eq. (A1)] of the i th component. Similarly,

$$C_c^{22}(t) = \langle \mathbf{S}_2(\tau) \cdot \mathbf{S}_2(\tau+t) \rangle - C^2(t), \quad (\text{C5})$$

$$C_c^{12}(t) = \left\langle \sum_{i=1}^{N_1} \sum_{j=1}^{N_2} \mathbf{v}_i(\tau) \cdot \mathbf{v}_j(\tau+t) \right\rangle_\tau \quad (\text{C6})$$

$$= \langle \mathbf{S}_1(\tau) \cdot \mathbf{S}_2(\tau+t) \rangle, \quad (\text{C7})$$

where $\mathbf{S}_2(\tau) = \sum_{i=1}^{N_2} \mathbf{v}_i(\tau)$. Equations (C4), (C5), and (C7) require a computational effort of $O(1)$ once the VACFs have been computed. These expressions also suggest that, unlike VACFs, VCCFs are collective properties.

-
- [1] J. Karger and D. M. Ruthven, *Diffusion in Zeolites and Other Microporous Solids* (Wiley, New York, 1992).
- [2] S. P. Bates and R. A. van Santen, *Adv. Catal.* **42**, 1 (1998).
- [3] R. M. Barrer, *Zeolites and Clay Minerals as Sorbents and Molecular Sieves* (Addison-Wesley, Reading, MA, 1978).
- [4] R. J. Bearman, *J. Phys. Chem.* **65**, 1961 (1961).
- [5] R. J. Bearman and J. G. Kirkwood, *J. Chem. Phys.* **28**, 136 (1958).
- [6] U. Balucani, R. Vallauri, and C. S. Murthy, *Phys. Lett.* **84A**, 133 (1981).
- [7] U. Balucani, R. Vallauri, and C. S. Murthy, *J. Chem. Phys.* **77**, 3233 (1982).
- [8] U. Balucani, *J. Phys. Chem.* **16**, 5605 (1983).
- [9] A. Verdaguer, J. A. Padro, and J. Trullas, *J. Chem. Phys.* **109**, 228 (1998).
- [10] U. Balucani, R. Vallauri, T. Gaskell, and M. Gori, *Phys. Lett.* **102A**, 109 (1984).
- [11] M. Schoen and C. Hoheisel, *Mol. Phys.* **52**, 33 (1984).
- [12] M. Schoen and C. Hoheisel, *Mol. Phys.* **52**, 1029 (1984).
- [13] H. P. van den Berg and C. Hoheisel, *Phys. Rev. A* **42**, 2090 (1990).
- [14] H. P. van den Berg and C. Hoheisel, *Phys. Rev. A* **42**, 3368 (1990).
- [15] J. Trullas and J. A. Padro, *Phys. Rev. E* **50**, 1162 (1994).
- [16] Y. Zhou and G. H. Miller, *Phys. Rev. E* **53**, 1587 (1996).
- [17] J. P. Hansen and I. R. M. Donald, *Phys. Rev. A* **11**, 2111 (1975).
- [18] J. P. Hansen and I. R. McDonald, *Theory of Simple Liquids* (Academic, London, 1976).
- [19] R. L. June, A. T. Bell, and D. N. Theodorou, *J. Phys. Chem.* **94**, 1508 (1990).
- [20] P. Demontis, G. B. Suffriti, and A. Tilocca, *J. Chem. Phys.* **105**, 5586 (1996).
- [21] A. V. Anil Kumar and S. Yashonath, *J. Phys. Chem. B* **104**, 9126 (2000).
- [22] S. M. Auerbach, N. J. Henson, A. K. Cheetam, and H. Metiu, *J. Phys. Chem.* **99**, 10 600 (1995).
- [23] S. Jost *et al.*, *J. Phys. Chem.* **102**, 6375 (1998).
- [24] R. Q. Snurr and J. Karger, *J. Phys. Chem. B* **101**, 6375 (1997).
- [25] D. L. Jolly and R. J. Bearman, *Mol. Phys.* **44**, 665 (1981).
- [26] M. J. Sanborn and R. Q. Snurr, *Sep. Purif. Technol.* **20**, 1 (2000).
- [27] S. R. de Groot and P. Mazur, *Non-Equilibrium Thermodynamics* (Dover, New York, 1984).
- [28] L. S. Darken, *Trans. AIME* **175**, 184 (1948).

- [29] H. Jobic, A. N. Fitch and A. Renouprez, *J. Phys. Chem.*, 1311 (1986).
- [30] P. Demontis, G. B. Suffritti, S. Quartieri, E. S. Fois, and A. Gamba, *J. Phys. Chem.* **92**, 867 (1988).
- [31] M. P. Allen and D. J. Tildesley, *Computer Simulation of Liquids* (Clarendon, Oxford, 1987).
- [32] F. O. Raineri and H. L. Friedman, *J. Chem. Phys.* **91**, 5633 (1989).
- [33] F. O. Raineri and H. L. Friedman, *J. Chem. Phys.* **91**, 5642 (1989).
- [34] C. Rajappa and S. Yashonath, *J. Phys. Chem. B* **101**, 5437 (1997).
- [35] W. W. Wood, in *Physics of Simple Liquids*, edited by H. N. V. Temperley, J. S. Rowlinson, and C. S. Rushbrooke (North Holland Publishing Co., Amsterdam, 1968), pp. 115–230.